

Integral refractive index determination of living suspension cells by multifocus digital holographic phase contrast microscopy

Björn Kemper
Sebastian Kosmeier
Patrik Langehanenberg
Gert von Bally

University of Muenster
Laboratory of Biophysics
Robert-Koch-Str. 45
D-48129 Muenster, Germany
E-mail: bkemper@uni-muenster.de

Ilona Bredebusch
Wolfram Domschke
Jürgen Schneckeburger

University of Muenster
Department of Medicine B
Albert-Schweitzer-Str. 33
D-48129 Muenster, Germany

Abstract. A method for the determination of the integral refractive index of living cells in suspension by digital holographic microscopy is described. Digital holographic phase contrast images of spherical cells in suspension are recorded, and the radius as well as the integral refractive index are determined by fitting the relation between cell thickness and phase distribution to the measured phase data. The algorithm only requires information about the refractive index of the suspension medium and the image scale of the microscope system. The specific digital holographic microscopy advantage of subsequent focus correction allows a simultaneous investigation of cells in different focus planes. Results obtained from human pancreas and liver tumor cells show that the integral cellular refractive index decreases with increasing cell radius. © 2007 Society of Photo-Optical Instrumentation Engineers. [DOI: 10.1117/1.2798639]

Keywords: digital holographic microscopy; refractive index determination; marker-free life cell analysis.

Paper 07042R received Feb. 4, 2007; revised manuscript received Jun. 9, 2007; accepted for publication Jun. 11, 2007; published online Oct. 19, 2007.

1 Introduction

Digital holographic microscopy¹⁻⁴ and interferometric phase contrast methods^{5,6} enable a quantitative marker-free dynamic analysis of living cells. Knowledge of the integral cellular refractive index allows the determination of the cell thickness and for adherently grown cells, the cell shape from the obtained phase contrast images.^{3,7} Previously published methods for the determination of the refractive index of single cells require a preparation of the sample,⁷ an exchange of the cell culture medium,⁸ or specific microfluidic equipment,^{9,10} which may affect the sample, is time consuming, or often not applicable. Here, a method for the determination of the cellular refractive index by digital holographic microscopy is described that requires only cells in suspension and a calibrated image scale. Therefore, the method is easy to handle and opens up an effective way of single-cell integral refractive index determination. The combination with the specific digital holographic microscopy feature of subsequent numerical focus correction provides increased data acquisition by simultaneous recording of cells in different focus planes.

2 Setup for Digital Holographic Microscopy

Figure 1 depicts the scheme of the applied digital holographic microscopy system. An inverse microscope arrangement enables the investigation of living cells in culture/buffer medium. Microscope lenses (Zeiss LD Achromat 40 × /0.6 Korr, Zeiss LD Neofluar 63 × /0.75 Korr) are applied

to magnify the object wave. The reconstruction of the digitally captured off-axis holograms is performed by a nondiffractive reconstruction method.^{2,11} Due to the applied algorithm, the reconstructed holographic images do not contain the disturbing terms “twin image” and “zero order.” Furthermore, a reconstruction of holograms with a sharply focused image of the sample is possible, which is of particular advantage for the alignment of the experimental setup.⁷

3 Refractive Index Determination of Spherical Cells in Suspension

The relation between the measured phase distribution $\Delta\varphi_{\text{cell}}$ that is affected by the cell thickness $d(x,y)$ in comparison to the surrounding buffer medium is:

$$\Delta\varphi_{\text{cell}}(x,y) = \frac{2\pi}{\lambda}(n_{\text{cell}} - n_{\text{medium}}) \cdot d(x,y), \quad (1)$$

with the integral cellular refractive index n_{cell} , the known homogenous refractive index of the buffer medium n_{medium} , and the wavelength λ of the applied laser light. For cells in suspension located at $x=x_0$, $y=y_0$ with a spherical shape and radius R (see Fig. 2), the cell thickness $d(x,y)$ is

Address all correspondence to Björn Kemper, Laboratory of Biophysics, University of Muenster, Robert-Koch-Str. 45 Muenster, NRW D-48129 Germany; Tel: 492-518-356888; Fax: 492-518-358536; E-mail: bkemper@uni-muenster.de

$$d(x,y) = \begin{cases} 2 \cdot [R^2 - (x-x_0)^2 - (y-y_0)^2]^{1/2} & \text{for } (x-x_0)^2 + (y-y_0)^2 \leq R^2 \\ 0 & \text{for } (x-x_0)^2 + (y-y_0)^2 > R^2 \end{cases} \quad (2)$$

Insertion of Eq. (1) into Eq. (2) yields:

$$\Delta\varphi_{\text{cell}}(x,y) = \begin{cases} \frac{4\pi}{\lambda} \cdot [R^2 - (x-x_0)^2 - (y-y_0)^2]^{1/2} \cdot (n_{\text{cell}} - n_{\text{medium}}) & \text{for } (x-x_0)^2 + (y-y_0)^2 \leq R^2 \\ 0 & \text{for } (x-x_0)^2 + (y-y_0)^2 > R^2 \end{cases} \quad (3)$$

with the unknown parameters n_{cell} , R , x_0 , and y_0 . For the described experiments, Eq. (3) is fitted line-wise in the x direction with the Gauß-Newton method¹² to the measured phase data of spherical suspension cells by iterative calculation of n_{cell} , $R_x(y) = [R^2 - (y-y_0)^2]^{1/2}$, and x_0 . The image scale was calibrated by a transparent USAF 1951 resolution test chart. Figure 3 illustrates the evaluation process by a representative result that has been obtained from a trypsinized human pancreas tumor cell (PaTu 8988 T) with spherical shape. The refractive index of the cell culture medium Dulbecco's modified eagle medium (DMEM) containing 5 % Fetal calf serum (FCS) and 5 % horse serum is determined to $n_{\text{medium}} = 1.337 \pm 0.001$ with an Abbe refractometer. Figure 3(a) shows the phase contrast image of the cell, coded to 256 gray levels (8 bit). The data $\Delta\varphi_{\text{cell}}(x,y)$ for the fitting process is selected by a threshold value that specifies the phase noise in the area around the cell. In Fig. 3(b), the fit of Eq. (3) to the data along the cross section in the x direction that is marked by the dashed line in Fig. 3(a) is depicted. Figures 3(c) and 3(d) represent the pseudo 3-D plots of the phase distribution in Fig. 3(a) in comparison to the same data achieved by the line-wise fitted data from Eq. (3). The mean value of the cell refractive index $n_{\text{cell}} = 1.372 \pm 0.002$ is used for further analysis. The uncertainty for n_{cell} is estimated by the standard deviation obtained from all line fits. The cell radius is obtained by determination of $R = R_x(v=v_0) \equiv R_{\text{fit,max}}$ from all fitted lines (for Fig. 3, $R_{\text{fit,max}} = 10.2 \pm 0.1 \mu\text{m}$). The uncertainty for R is calculated by the standard deviation of ± 5 neighboring lines to the central line at $R = R_{\text{fit,max}}$. Figure 3(e) shows the

absolute values of the phase difference between the measured phase contrast data in Fig. 3(c) and the fitted data in Fig. 3(d) (mean value = 0.3 rad), which indicates a homogeneous distribution of the fitting errors.

4 Results

First, investigations on simulated phase data of cells with a constant refractive index ($n_{\text{cell,sim}} = 1.38$) and different cell radii ($R = 0.5 - 10 \mu\text{m}$, $N = 64$) according to Eq. (3) were carried out to determine the resolution of the described fit-algorithm for refractive index measurement. For all simulations, a cell radius independent refractive index $n_{\text{cell,sim}} = 1.38001 \pm 0.00001$ was obtained. Further experiments on homogeneous beads (Cytodex™ 1, GE Healthcare, Germany, $N = 27$) in water ($n_{\text{water}} = 1.334 \pm 0.001$) resulted in a radius independent refractive index $n_{\text{cell,beads}} = 1.3377 \pm 0.0004$.

Three different human pancreas tumor cell lines^{13,14} [PaTu 8988 T ($N = 28$), PaTu 8988 S ($N = 15$), and PaTu 8988 T pLXIN E-Cadherin ($N = 20$)] were investigated in comparison to a human liver tumor cell line¹⁵ (HepG2, $N = 55$). The cells were trypsinized, and for each cell line, the parameters n_{cell} and $R_{\text{fit,max}}$ were determined with the described algorithm ($n_{\text{medium}} = 1.337 \pm 0.001$). For data evaluation, only cells with spherical shape were selected, which were observed in the main fraction of the recorded holographic phase contrast images for all investigated cell lines. Figures 4(a) and 4(b) depict the refractive index n_{cell} in dependence of $R_{\text{fit,max}}$ for pancreas and liver tumor cells. Within the range of uncertainty, no significant differences between the data of the three different types of pancreas tumor cells are observed [Fig. 4(a)]. Furthermore, Fig. 4(a) shows that the cellular refractive index of the cells decreases with increasing $R_{\text{fit,max}}$. The data obtained from the liver tumor cells [Fig. 4(b)] shows the same behavior. For the pancreas tumor cells, the mean refractive

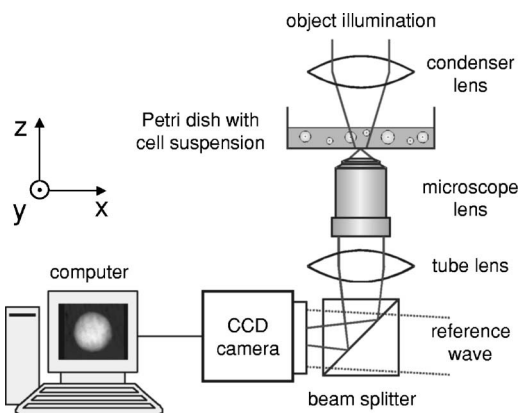


Fig. 1 Scheme for an inverse off-axis digital holographic microscopy setup with frequency-doubled Nd:YAG laser ($\lambda = 532 \text{ nm}$).

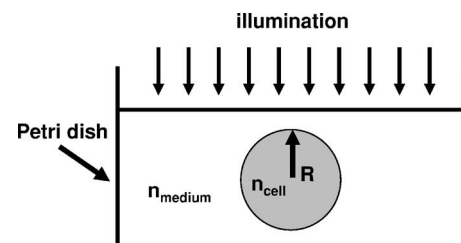


Fig. 2 Principle for refractive index determination of spherical cells in suspension. R is the cell radius; n_{cell} the integral cellular refractive index; and n_{medium} the refractive index of the buffer medium.

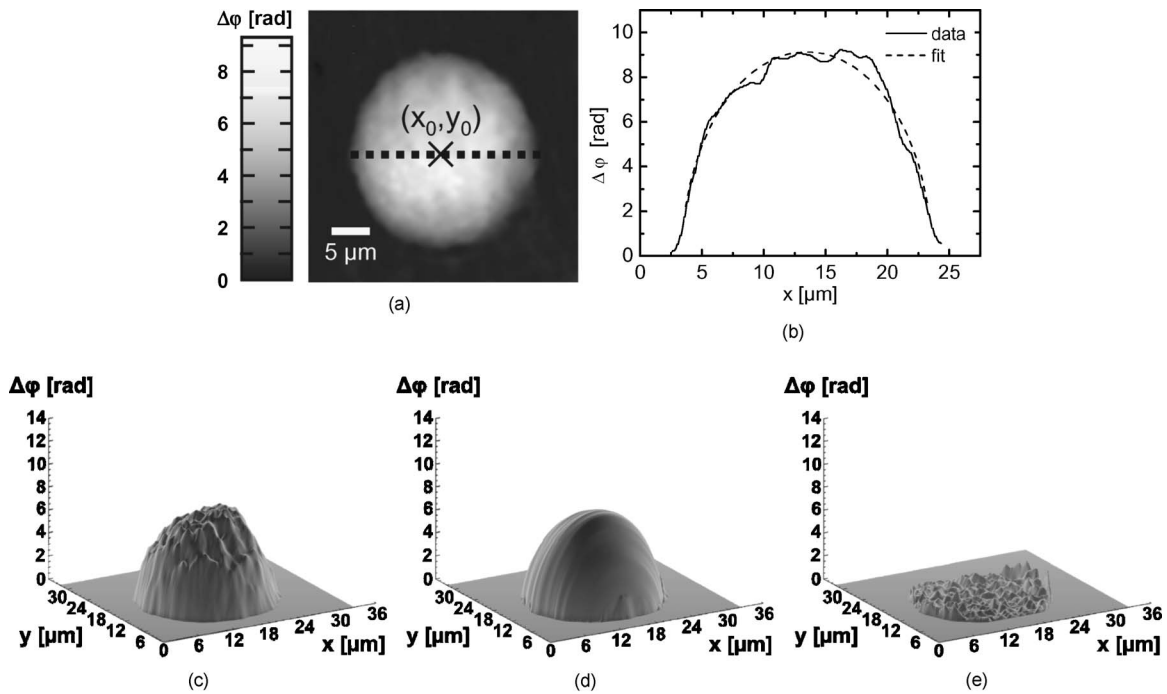


Fig. 3 Refractive index determination of suspension cells: (a) reconstructed quantitative digital holographic phase contrast image of a spherical trypsinized pancreas tumor cell located at (x_0, y_0) ; (b) phase data $\Delta\phi$ along the cross section marked by the dashed line in (a) and the fitted data corresponding to Eq. (3); (c) rendered pseudo 3-D plot of the phase distribution in (a) that is used for the determination of the integral refractive index; (d) rendered pseudo 3-D plot of data that is obtained by line-wise fitting of Eq. (3); (e) rendered pseudo 3-D plot of the phase difference data between (c) and (d).

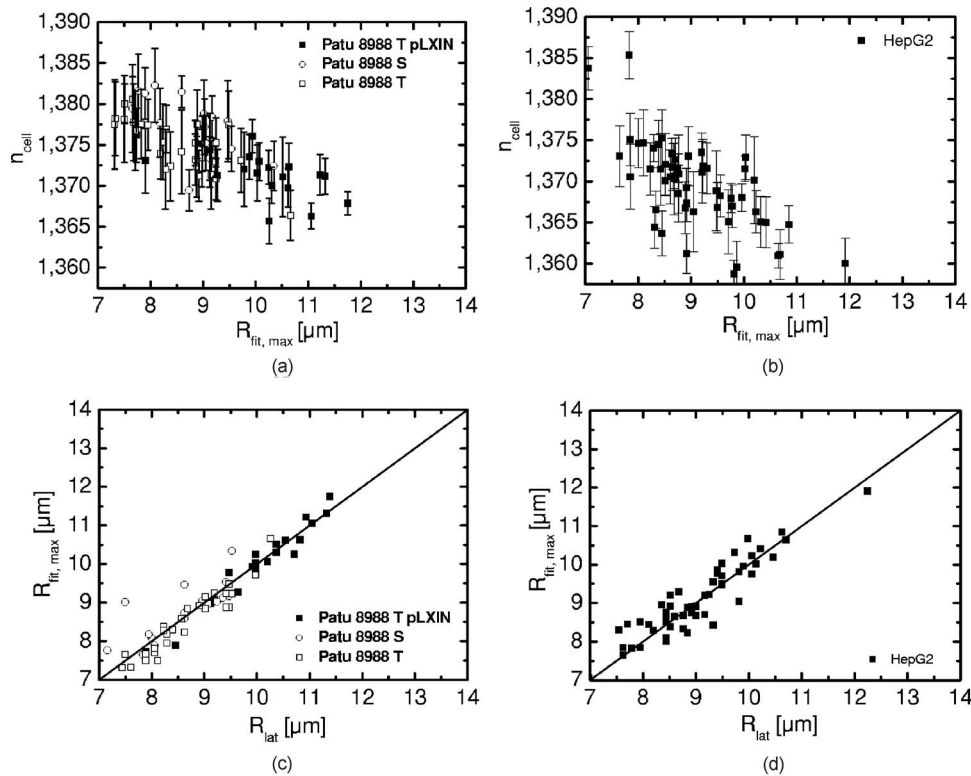


Fig. 4 Refractive index determination of PaTu 8988 XX cells and HepG2 cells. (a) and (b) Integral cellular refractive index n_{cell} of PaTu 8988 XX cells and HepG2 cells versus the cell radius $R_{\text{fit,max}}$ obtained from the fit of Eq. (3). (c) and (d) Cell radius $R_{\text{fit,max}}$ obtained from Eq. (3) versus the cell radius R_{lat} that is determined from the lateral image scale for both PaTu 8988 XX cells and HepG2 cells.

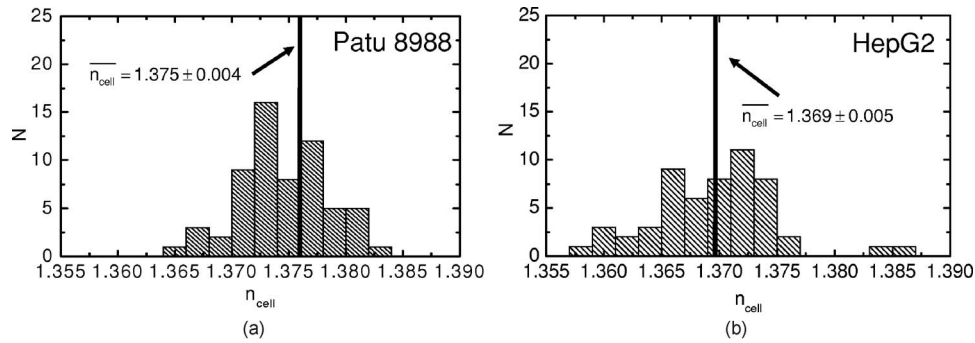


Fig. 5 Histogram of the refractive index data for (a) PaTu 8988 XX cells and (b) HepG2 cells.

index determined to $\overline{n_{\text{cell}}}=1.375\pm 0.004$ for a mean cell radius $R_{\text{fit,max}}=9.1\pm 1.1$, while for the liver tumor cells $n_{\text{cell}}=1.369\pm 0.005$ with $R_{\text{fit,max}}=9.1\pm 0.9$ is obtained. To verify the fitting process, the cell radius $R_{\text{fit,max}}$ is plotted versus the radius R_{lat} of the cells that is determined from the phase contrast images by the image scale. The results are shown in Figs. 4(c) and 4(d) for PaTu 8988 XX and HepG2 cells. A proportional relation is obtained that is in correspondence with the results of the fitting algorithm. The decrease of the refractive index with increasing cell radius, and thus the cell volume, may be explained by cellular water content.¹⁶ Figures 5(a) and 5(b) show the histogram plots of the refractive index for both cell lines. The maximum numbers of cells is located near the mean value of the refractive index.

5 Conclusions

In summary, an algorithm for the marker-free retrieval of the integral refractive index of living cells from digital holographic phase contrast images is presented that can be applied to cell lines with a mainly spherical shape, like the investigated trypsinized PaTu 8988 XX and HepG2 tumor cells in suspension. The mean error for n_{cell} is determined to 0.005. The algorithm allows a refractive index analysis of cells without additional sample preparation. Due to the multifocus ability of digital holographic microscopy, an increased data acquisition can be achieved by simultaneous recording of cells located in different focal planes of the suspension. Furthermore, it is demonstrated that the integral refractive index of cells depends on the cell size. This information is important, e.g., for the utilization of optical tweezers and related optical manipulation systems, where the individual cellular refractive index represents a parameter for calculation of the applied forces.¹⁷⁻¹⁹ In addition, the method opens up new perspectives for the quantitative monitoring of cell swelling processes.¹⁶ Here, e.g., water absorption/permeability effects a decrease of the cellular refractive index that leads to an underestimation of the cell thickness in digital holographic phase contrast microscopy due to Eq. (1). In this way, the precision of such measurements can be significantly improved. In conclusion, the proposed method allows the application of digital holographic microscopy in an enhanced variety of life cell analytical approaches.

Acknowledgments

The authors acknowledge financial support by the German Federal Ministry of Education and Research (BMBF) and Deutsche Forschungsgemeinschaft (DFG), and thank Andreas Bauwens, Institute of Medical Physics and Biophysics, University of Muenster, Germany, for the support during the experiments with the beads.

References

1. E. Cuche, P. Marquet, and C. Depeursinge, "Simultaneous amplitude-contrast and quantitative phase-contrast microscopy by numerical reconstruction of Fresnel off-axis holograms," *Appl. Opt.* **38**, 6994–7001 (1999).
2. D. Carl, B. Kemper, G. Wernicke, and G. von Bally, "Parameter-optimized digital holographic microscope for high-resolution living cell analysis," *Appl. Opt.* **43**, 6536–6544 (2004).
3. P. Marquet, B. Rappaz, P. J. Magistretti, E. Cuche, Y. Emery, T. Colomb, and C. Depeursinge, "Digital holographic microscopy: a noninvasive contrast imaging technique allowing quantitative visualization of living cells with sub wavelength accuracy," *Opt. Lett.* **30**, 468–470 (2005).
4. C. J. Mann, L. Yu, C. M. Lo, and M. K. Kim, "High-resolution quantitative phase-contrast microscopy by digital holography," *Opt. Express* **13**, 8693–8698 (2005).
5. G. Popescu, L. Deflores, J. C. Vanghan, K. Badizadegan, H. Iwai, R. R. Dasari, and M. S. Feld, "Fourier phase microscopy for investigations of biological structures and dynamics," *Opt. Lett.* **29**, 2503–2505 (2004).
6. T. Ikeda, P. Popescu, P. Dasari, and M. S. Feld, "Hilbert phase microscopy for investigating fast dynamics in transparent systems," *Opt. Lett.* **30**, 1165–1167 (2005).
7. B. Kemper, D. Carl, J. Schnekenburger, I. Bredebusch, M. Schäfer, W. Domschke, and G. von Bally, "Investigations on living pancreas tumor cells by digital holographic microscopy," *J. Biomed. Opt.* **11**, 034005 (2006).
8. B. Rappaz, P. Marquet, E. Cuche, Y. Emery, C. Depeursinge, and P. J. Magistretti, "Measurement of the integral refractive index and dynamic cell morphometry of living cells with digital holographic microscopy," *Opt. Express* **13**, 9361–9373 (2005).
9. X. J. Liang, A. Q. Liu, X. M. Zhang, P. H. Yap, T. C. Ayi, and H. S. Yoon, "Determination of refractive index for single living cell using integrated biochip," *Digest Tech. Papers Transducers '05, 13th Intl. Conf. Solid-State Sensors, Actuators Microsyst.*, **2**, 1712–1715 (2005).
10. W. Z. Zhong, X. M. Zhang, A. Q. Liu, C. S. Lim, P. H. Yap, and H. M. M. Hosseini, "Refractive index measurement of single living cells using on-chip Fabry-Pérot cavity," *Appl. Phys. Lett.* **89**, 203901 (2006).
11. M. Liebling, T. Blu, and M. Unser, "Complex-wave retrieval from a single off-axis hologram," *J. Opt. Soc. Am. A* **21**, 367–377 (2004).
12. Å. Björk, *Numerical Methods for Least Squares Problems*, Society of Industrial & Applied Mathematics, Philadelphia, PA (1996).

13. H. P. Elsässer, U. Lehr, B. Agricola, and H. F. Kern, "Establishment and characterization of two cell lines with different grade of differentiation derived from one primary human pancreatic adenocarcinoma," *Virchows Arch. B* **61**, 295–306 (1992).
14. J. Schnekenburger, J. Mayerle, B. Krüger, I. Buchwalow, F. U. Weiss, E. Albrecht, V. E. Samoilova, W. Domschke, and M. M. Lerch, "Protein tyrosine phosphatase k and SHP-1 are involved in the regulation of cell-cell contacts at adherens junctions in the exocrine pancreas," *Gut* **54**, 1445–1455 (2005).
15. D. P. Aden, A. Fogel, S. Plotkin, I. Damjanov, and B. B. Knowles, "Controlled synthesis of HBsAg in a different human liver carcinoma-derived cell line," *Nature (London)* **282**, 615–616 (1979).
16. J. Farinas and A. S. Verkman, "Cell volume and plasma membrane osmotic permeability in epithelial cell layers measured by interferometry," *Biophys. J.* **71**, 3511–3522 (1996).
17. A. Ashkin, "Optical trapping and manipulation of neutral particles using lasers," *Proc. Natl. Acad. Sci. U.S.A.* **94**, 4853–4860 (1997).
18. J. Guck, R. Ananthakrishnan, T. J. Moon, C. C. Cunningham, and J. Käs, "The optical stretcher—a novel, noninvasive tool to manipulate biological materials," *Biophys. J.* **81**, 767–784 (2001).
19. Z. Hu, J. Wang, and J. Liang, "Manipulation and arrangement of biological and dielectric particles by a lensed fiber probe," *Opt. Express* **12**, 4123–4128 (2004).